Synthesis of reactive MgO from reject brine via the addition of NH_4OH

Haoliang Dong[a], Cise Unluer[a], En-Hua Yang[a,*], Abir Al-Tabbaa[b]

[a]School of Civil and Environmental Engineering, Nanyang Technological University, 50 Nanyang Avenue, Singapore 639798, Singapore

[b]Department of Engineering, University of Cambridge, Trumpington Street, Cambridge CB2 1PZ, UK

Abstract

Reactive magnesia (MgO) with a high purity and reactivity is used in several high-end applications. This study reports the feasibility of synthesizing high reactivity MgO from reject brine with the use of NH_4OH. The molar amount of NH_4OH was optimized at a NH_4OH /Mg^{2+} molar ratio of 6 to provide maximum magnesium oxide yield and purity. This led to the synthesis of $Mg(OH)_2$ with a purity of 93.5%, which was further calcined at 500 °C for 2 hours to produce reactive MgO with a SSA of 78.8 m^2/g. This study shed light on the significant potential of reject brine in the recovery of Mg^{2+} and the synthesis of reactive MgO with a wide range of potential applications.

Keywords: MgO; $Mg(OH)_2$; reject brine; NH_4OH; synthesis; microstructure

*Corresponding author. Address: N1-01b-56, 50 Nanyang Avenue, Singapore 639798. Tel.: +65 6790 5291; fax: +65 6791 0676. *E-mail address:* ehyang@ntu.edu.sg (E.H. Yang)

1. Introduction

Magnesium oxide (MgO) is produced in different grades and finds use in several applications ranging from the pharmaceutical to the refractory industries due to its superior stability and chemical resistance. A majority of MgO is produced via the calcination of magnesite ($MgCO_3$) through the dry route. The properties of the resulting MgO strongly depend on the calcination conditions. Higher calcination temperatures and longer residence times lead to increases in the size of the MgO grain, which results in the decrease of its specific surface area (SSA) and reactivity (Shand, 2006; Mo et al., 2010). Most of the commercially available MgO can be classified into four grades, depending on the conditions used during its production, i.e. calcination temperature and residence time. Fused MgO is produced above the fusion temperature of MgO (2800 °C) and has the lowest SSA and reactivity, which is excellent in chemical stability and moisture resistance (Wang et al., 2012). Dead-burned MgO is obtained at calcination temperatures above 1400 °C and has a very low SSA and reactivity. It is widely used in the refractory industry as a fire-resistant and thermal insulation material. Hard-burned MgO is produced at 1000-1400 °C with a low SSA and limited reactivity. It is mostly used as an expansive additive in concrete for shrinkage compensation (Gao et al., 2008; Mo et al., 2014). Light-burned (reactive or caustic-calcined) MgO is produced at much lower temperatures ranging between 700 and 1000 °C and therefore retains a high SSA and reactivity. Because of its high reactivity, the light-burned MgO has been used in various applications as a fertilisers, catalyst, chemical absorbent and filtration medium (Kramer, 2001; Lee et al., 2004; Shand, 2006; Caraballo et al., 2009). Recent studies have shown that reactive MgO can also be used as a cement binder by itself or along with Portland cement (PC) and other supplementary cementitious materials, depending on the application (Liska et al., 2012a; Liska et al., 2012b; Al-Tabbaa, 2013; Unluer and Al-Tabbaa, 2013; Unluer and Al-

Tabbaa, 2014). The main advantages of reactive MgO cements over traditional PC are listed as its significantly lower calcination temperatures (700-1000 vs. 1450 °C), ability to absorb carbon dioxide (CO_2) in the form of stable carbonates while gaining strength, and complete recyclability at the end of its lifetime.

Unlike limestone which is abundant and available worldwide, large magnesite deposits are mainly located in China and North Korea (Shand, 2006). According to RAM (2015), around 8.5 million tonnes of MgO is produced from magnesite annually, for which China is the leading provider with a 49% market share. Lack of magnesite availability on a global level highlights the need to identify alternative sources for the production of MgO, which also suffers from low purity and reactivity due to the impurities present in the parent materials. Today, a significant portion of global MgO supply is via the calcination of magnesium hydroxide $Mg(OH)_2$ generated from magnesium-rich sources such as seawater or natural brine, which contributes to about 14% of the global MgO production (Kramer, 2001). This process involves the extraction of seawater/brine, pre-treatment and final processing steps. Seawater intake structures are mostly utilized in large seawater desalination plants which mainly extract seawater from open sea (Pankratz, 2004). Seawater/brine pre-treatment often employs a pH adjuster to de-carbonate the solution at hand. This involves the addition of sulphuric acid to decrease the pH of the solution to 4. Seawater is then passed through a desorption tower where it is aerated to remove CO_2 in case of the precipitation of $CaCO_3$ along with $Mg(OH)_2$ (Shand, 2006). After the seawater/brine is softened, it is then pumped into an agitated reactor vessel, during which a strong base is added into the solution to raise the pH to 10.5, enabling the precipitation of magnesium (Shand, 2006). Generally, calcium

hydroxide ($Ca(OH)_2$) derived from calcined lime (CaO) or dolime (CaO·MgO) is deployed in practice. Friedrich et al. (1946) patented a simple process to precipitate MgO in the form of $Mg(OH)_2$ from seawater at a pH of 10.5 using a lime solution (Friedrich et al., 1946). Dolime is preferred due to its self-contained MgO content, enabling the use of only half of the usually required volume of seawater or brine while the other half is derived from dolime to produce the same amount of MgO as would be if lime was used (Al-Zahrani and Abdel-Majeed, 2007).

The precipitation of Mg^{2+} can be performed via the addition of a range of alkali sources other than lime (Turek and Gnot, 1995; Dave and Ghosh, 2005; El-Naas, 2011; Tran et al., 2013; Khuyen Thi et al., 2016). Hydrated lime ($Ca(OH)_2·2H_2O$) can also be used to precipitate $Mg(OH)_2$ from seawater at a pH ranging between 7 and 7.5 (Dave and Ghosh, 2005). However the introduction of calcium-based alkalis results in the formation of gypsum ($CaSO_4·2H_2O$) along with other precipitates due to the presence of sulphate in seawater, which necessitates the pre-treatment of seawater by adding $CaCl_2$ for desulfation. Another additive utilized for the precipitation of $Mg(OH)_2$ from natural mine brine is sodium hydroxide (NaOH). Turek and Gnot (1995) explored the effect of reaction temperature on the sedimentation of the precipitants via the addition of NaOH into mine brine, which found out the improved precipitation when reaction temperature decreased from 40 to 10 °C. The improved sedimentation was attributed to the high viscosity of NaOH solution and brine, which impeded the contact between the precipitating agent and mine brine and lowered the diffusion rate, thereby improving the crystal structure of $Mg(OH)_2$ (Turek and Gnot, 1995). Ammonia solution (NH_4OH) has also been reported to precipitate $Mg(OH)_2$ from seawater/brine. The use of NH_4OH buffers the solution at a basic pH of around 10, which

favours the precipitation of $Mg(OH)_2$. Unlike other alkalis such as lime or dolime, NH_4OH does not introduce additional cations which result in undesirable precipitates (e.g. $CaCO_3$), as impurities. Furthermore, NH_4OH can be recycled at the end of the reaction, which allows the design of a closed-system as suggested in the modified Solvay process and thereby eliminates the generation of waste (El-Naas, 2011).

The precipitation of Mg^{2+} from synthetic solutions has also been performed by several studies (Alvarado et al., 2000; Henrist et al., 2003; Yan et al., 2005). Henrist et al. (2003) studied the influence of the chemical nature of the utilized bases (NaOH and NH_4OH), type of counter-ions and temperature on the morphological characteristics of $Mg(OH)_2$ precipitated from a synthetic $MgCl_2$ solution. It was observed that the use of NaOH as the alkali source led to the formation of $Mg(OH)_2$ with a globular cauliflower-like morphology, which consisted of small particles with dispersed agglomerates; while the use of NH_4OH as the alkali source resulted in a plate-like $Mg(OH)_2$ morphology. Single and circular plate-like particles were observed at lower temperatures while particles had a tendency to inter-grow at 60 °C (Henrist et al., 2003). Yan et al. (2005) reported the synthesis of $Mg(OH)_2$ nano-flowers by a simple hydrothermal reaction of $MgCl_2$ and $CO(NH_2)_2$ without any additives. The pH of the magnesium chloride solution was first adjusted at a range of 3.0-9.5 via the addition of HCl or NH_4OH. The solution was then sealed in an autoclave at 95-130 °C for 18 hours before collecting the samples. It was found that the pH value and temperature during the initial reaction was essential in controlling the morphology of particles. The initially irregular spherical particles developed a nano-flower morphology with increasing pH and temperature. This was attributed to the stacking of excessive Mg^{2+} and OH^- on the existing plate-like crystal seeds and therefore self-assembling into a flower like structure at high pH values (Yan et al., 2005).

Calcination of the resulting $Mg(OH)_2$ synthesized from seawater/brine or synthetic solutions produces MgO (Friedrich et al., 1946; Shand, 2006). A number of studies have investigated the properties of MgO calcined from $Mg(OH)_2$ (Eubank, 1951; Itatani et al., 1988; Choudhary et al., 1994; Alvarado et al., 2000; Bartley et al., 2012). Eubank (1951) identified that the reaction temperature and presence of impurities significantly influence the properties of MgO. The calcination of magnesium compounds was reported to take place in two distinct stages starting with the loss of water and CO_2 gases between 300 and 500 ºC, which creates a porous structure. Recrystallization or sintering takes place at higher temperatures (> 900 ºC), densifying the final material, whose porosity decreases during this process. The particle sizes of calcined MgO increase with increasing calcination temperature, resulting in the decrease of surface area and adsorptive capacity (Eubank, 1951). The impurities contained in MgO can enhance the sintering process through the formation of vitreous phases. Alvarado et al. (2000) characterised MgO prepared from three precursor magnesium salts and dolomite (Alvarado et al., 2000). The SSA of calcined MgO from different magnesium compounds precursors were found in the decreasing order: magnesium sulfate > magnesium nitrate > magnesium acetate > dolomite. On the contrary, the particle size, degree of agglomeration and porosity displayed the inverse sequence.

The main difference between MgO obtained from the calcination of magnesite and synthetically from seawater/brine or any relevant solutions is the higher purity and reactivity of the latter (Jin and Al-Tabbaa, 2014). The main drawback of the production of MgO from seawater/brine is its higher energy consumption when compared to the dry route (17 vs. 5.9 GJ per tonne of MgO (Hassan, 2013)). However, this can be optimized as further studies are

performed on the reduction of the energy demands of MgO production from waste brine. This is particularly critical for coastal regions with a limited amount of fresh water resources such as Singapore, where desalination is considered as a feasible approach to meet residential and industrial water demands. Desalination involves the removal of salts from saline water to produce fresh water. Currently the desalinated water from two current running seawater reverse-osmosis plants provides 100 million gallons water a day, which meets up to 25% of Singapore's current water demand (PUB, 2015). According to the International Desalination Association, the global daily production of desalinated water generated by 18,426 desalination plants worldwide exceeds 86.8 million cubic meters (IDA, 2015). It is estimated that an equivalent amount is generated as reject brine per m^3 of desalinated water (El-Naas, 2011).

Reject brine, which is of particular interest in this study, is a concentrated by-product with a high salt concentration obtained from treating brackish water or seawater in desalination plants (Adham et al., 2013). The most common way to dispose reject brine is through its discharge back to the sea. However, reject brine is denser than the feedstock supply due to its high salt concentration and salinity and therefore tends to accumulate at the bottom of the sea when discharged through an outfall without sufficient mixing. Discharge of untreated reject brine has an adverse effect on the ecosystem as it alters the flora and fauna through increased salinity and directly or indirectly damages all living organisms within that particular ecosystem (Mohamed et al., 2005). A newly proposed alternative is the re-treatment of the salt within the reject brine to obtain valuable materials such as Mg^{2+}, which can serve as an excellent source for the recovery of MgO. Therefore, reject brine can be converted into

valuable and useful solids, which provides a feasible and environmental friendly use of this waste material (El-Naas, 2011).

Although there are many studies on the reaction of synthetic $MgCl_2$ solution, seawater or natural brine with different alkali sources (Turek and Gnot, 1995; Henrist et al., 2003; Dave and Ghosh, 2005; Yan et al., 2005), limited research has been reported on the recovery of valuable metals from actual reject brine obtained from desalination plant (Ahmed et al., 2003). This paper reports the feasibility of synthesizing reactive MgO from reject brine collected from a local desalination plant in Singapore. A comprehensive study on the reaction kinetics and the physical and chemical properties of the resulting $Mg(OH)_2$ and MgO was performed via XRD, FESEM, TG/DTA and BET analyses.

2. Materials and Methodology

2.1. Materials

In this study, NH_4OH solution with analytical grade (25.0% NH_3 content) supplied by Sigma-Aldrich (Singapore) was used as the alkali source to react with reject brine. The reject brine was collected from the Tuaspring desalination plant in Singapore, the largest desalination plant in South East Asia with a capacity of 318,500 m^3 desalinated water per day. During the desalination process, ultra-filtration membrane technology is used to remove the suspended solids and microorganisms in the seawater intake during the pre-treatment process, which is followed by a two-stage seawater reverse osmosis process. Saline feed water (seawater) is passed through semi-permeable membranes to produce a low-salinity water and a very saline concentrate (reject brine) as a by-product, which would normally be disposed back to the sea through an outfall pipe (Hyflux, 2011).

Unlike seawater or natural brine, reject brine contains suspended solids through the chemicals added to precipitate the colloidal particles in the seawater before running through ultra-filtration in the desalination process. After the collection of reject brine from the plant, it was filtrated through a 45 μm membrane filter to remove suspended solids before further analysis. The chemical composition of the filtrated reject brine, determined via Inductively Coupled Plasma-Optical Emission Spectroscopy (ICP-OES), is summarized in Table 1. Along with a Mg^{2+} concentration of 1679 ppm, the presence of other impurities (e.g. Na^{+}, K^{+} and Ca^{2+}) was observed.

Table 1 Chemical composition of the reject brine used in this study

Element/ Concentration	Na	Mg	K	Ca	Sr	B	Si	Li	P	Al
PPM	16124.3	1679.0	808.5	563.6	5.3	4.5	0.5	0.4	0.2	0.1

2.2. Methodology

A pre-determined amount of NH_4OH (2.12-19.08 ml) was introduced into 200 ml of reject brine as the alkaline source to investigate the influence of NH_4OH dosage on the reaction kinetics with reject brine and the chemical and physical properties of the resulting $Mg(OH)_2$ precipitates. According to stoichiometry, the reaction of 2 moles of OH^- with 1 mole of Mg^{2+} leads to the precipitation of 1 mole of $Mg(OH)_2$. However, a higher dosage of NH_4OH (up to 19.08 ml) had to be utilized so that supersaturation can be reached due to its relatively weak nature ($K_b=1.8\times10^{-5}$) as a base.

Reject brine and NH_4OH solution were mixed with a magnetic stirrer at a constant stirring speed (300 rpm) and room temperature (25 °C), during which a pH/thermometer probe was inserted into the beaker to monitor the temperature and pH of the reaction. The experiment was terminated after 6 hours of reaction when the pH of the solution stabilized. The solids were then separated from the liquid phase through a centrifuge. Precipitates were collected and washed by ultrapure water for three times. The resulting precipitates ($Mg(OH)_2$) were oven-dried at 105 °C until they reached a constant mass. They were then ground into powder form passing through a 125 μm sieve, after which their chemical and physical properties were determined. The remaining precipitates were calcined at a pre-determined temperature of 500 °C for 2 hours in the furnace to produce reactive MgO, which was then characterized for its chemical and physical properties.

The pH and temperature of the reaction were monitored by using a pH/thermometer (Mettler Toledo pH/Ion meter S220), which was calibrated before each experiment with a standard solution set at a pH of 4, 7 and 10.21, to reveal the kinetics of the chemical reactions between reject brine and NH_4OH. Mg^{2+} and Ca^{2+} ion concentrations present in the solution after the completion of the reaction were monitored by means of an ICP-OES (PerkinElmer Optima DV2000) to determine the percentage of sequestrated ions. This provided insights on the yield of $Mg(OH)_2$ and $CaCO_3$ obtained at different levels of NH_4OH addition. The solution was diluted 10 times and filtrated through a 45 μm membrane filter to remove suspended solids. 1 ml of the reject brine/ NH_4OH solution (after the reaction) was then taken using a pipette and added to a 10 ml acidized solution (70% nitric acid) to fully terminate the reaction. The primary Na^+, Mg^{2+} and Ca^{2+} solutions with concentrations of 100 ppm were used for calibration before each of the ICP-OES measurements.

Several techniques including X-ray powder diffraction (XRD), field emission scanning electron microscopy (FESEM), thermogravimetric and differential thermal analysis (TG/DTA) and Brunauer-Emmett-Teller (BET) analyses were utilized to characterize the synthesized $Mg(OH)_2$ and reactive MgO. In preparation for these analyses, all samples were vacuum dried to constant mass, followed by grinding and sieving to achieve a particle size smaller than 125 µm. XRD was performed via a Bruker D8 Advance with a Cu Kα source under the operation conditions of 40 Kv and 40 mA, emitting radiation with a wavelength of 1.5405 Å, scan rate of 0.02 °/step, and a 2θ range of 5 to 70°. The morphology and microstructure of the synthesized samples were studied by imaging powder surface using a JSM-7600F thermal FESEM. Quantitative analysis of the phases in the synthesized samples was performed via TG/DTA using a PyrisDiamond TGA 4000 operated at a heating rate of 10 °C/min under air flow. The SSA of the synthesized samples was analysed through the BET analysis from nitrogen adsorption-desorption isotherms using a Quadrasorb Evo automated surface area and pore size analyser.

3. Results and Discussion

3.1. Reaction kinetics

Fig. 1 shows the change in pH over time during the reaction between reject brine and NH_4OH. The rate of change of pH recorded at regular intervals revealed the kinetics of the reaction under different amounts of NH_4OH. The general trend shows a steady pH after the addition of NH_4OH, followed by a gradual decrease that stabilized at a constant level when the reaction reached equilibrium. Both the initial and final pH values increased with the increase of NH_4OH dosage as more OH^- was available, which increased the reaction rate and shortened

the reaction time. This enabled the time needed to achieve equilibrium to reduce significantly from 240 to 25 minutes as the amount of NH_4OH increased from 2.12 to 19.08 ml, as shown in Fig. 2.

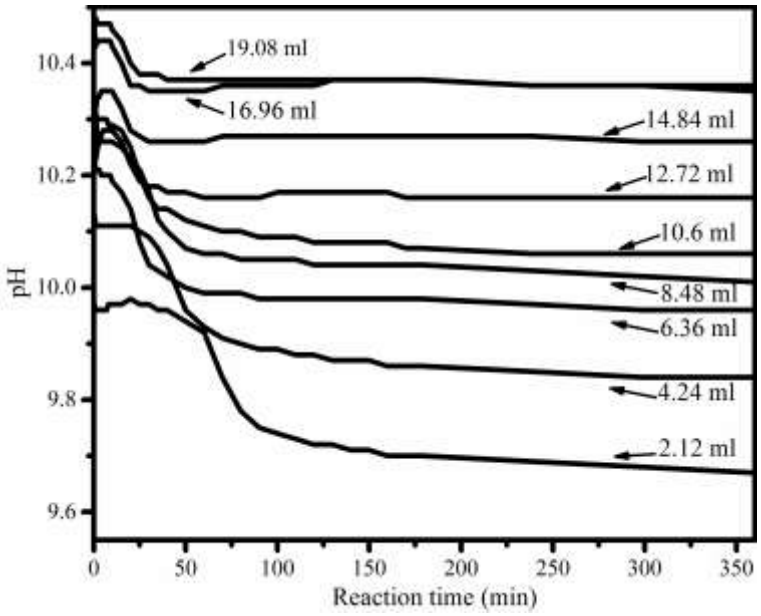

Fig. 1. pH of the reaction of reject brine with different amounts of NH_4OH

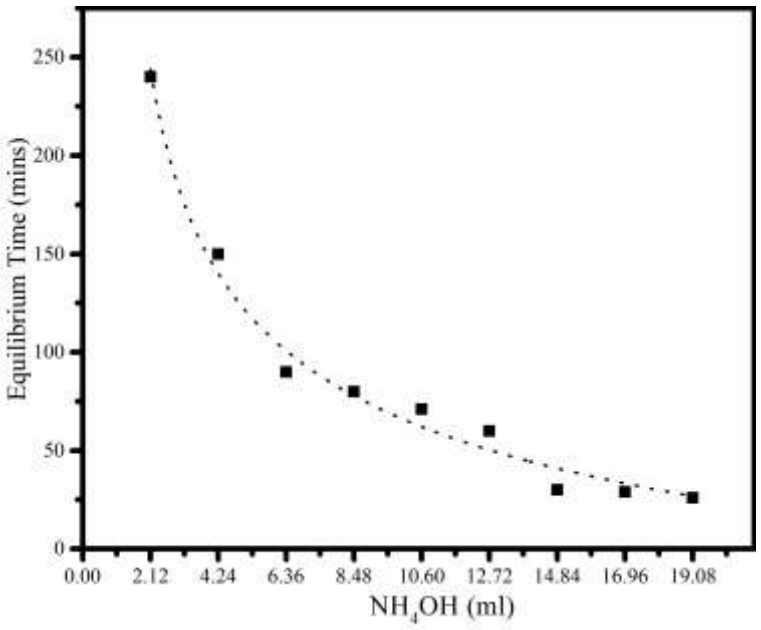

Fig. 2. Equilibrium time as a function of NH_4OH dosage

3.2. Recovery of Mg^{2+} and Ca^{2+} from reject brine

The formation of $Mg(OH)_2$ was observed via the reaction between the Mg^{2+} in the reject brine and OH^- provided by NH_4OH. The addition of NH_4OH also favoured the conversion of HCO^{3-} (origin from CO_2 in air dissolved in the reject brine) to CO_3^{2-}. This led to a reaction of CO_3^{2-} with Ca^{2+} and resulted in the precipitation of $CaCO_3$. The reaction paths observed during this process are shown in Eqns. 1 to 4 (Shand, 2006).

$$NH_4OH_{(aq)} \leftrightarrow NH_4^+ + OH^- \quad (1)$$

$$Mg^{2+} + 2OH^- \rightarrow Mg(OH)_2 \quad (2)$$

$$NH_4OH_{(aq)} + HCO_3^- \leftrightarrow CO_3^{2-} + NH_4^+ + H_2O \quad (3)$$

$$Ca^{2+} + CO_3^{2-} \rightarrow CaCO_3 \quad (4)$$

Fig. 3 shows the molar percentage of Mg^{2+} and Ca^{2+} recovered from reject brine through the addition of different amount of NH_4OH, which was calculated by measuring the ion concentration in the reject brine both before and after the reaction. The amount of Mg^{2+} and Ca^{2+} precipitated from the reject brine increased with the amount of NH_4OH addition. The precipitation of Mg^{2+} took place earlier than Ca^{2+} due to lower solubility product constant of $Mg(OH)_2$ (1.8×10^{-11} mol^3 l^{-3}) than that of $CaCO_3$ (3.8×10^{-9} mol^2 l^{-2}) (Sillén et al., 1964). In addition, the ion product $[Mg^{2+}][OH^-]^2$ was calculated to be 7×10^{-10} mol^3 l^{-3} at pH 10 (Fig. 1), which was larger than the solubility product constant of $Mg(OH)_2$ (1.8×10^{-11} mol^3 l^{-3}) (Sillén et al., 1964). This caused supersaturation of $Mg(OH)_2$ and enabled the reaction between OH^- with Mg^{2+} to precipitate $Mg(OH)_2$. As can be seen, precipitation of $CaCO_3$ was hindered at lower NH_4OH dosage (< 6.36 ml). This may be attributed to the lower pH of the solution,

which was unfavourable the conversion of HCO_3^- to CO_3^{2-} and the formation of $CaCO_3$, when less NH_4OH was added. Therefore, a higher content of Mg^{2+} than Ca^{2+} was precipitated when a lower amount of NH_4OH (< 6.36 ml) was used. As the amount of NH_4OH increased beyond 6.36 ml, the increased amount of OH^- in the solution achieved a sufficient level to react with both Mg^{2+}, CO_3^{2-} and Ca^{2+}, thereby increasing the amount of $CaCO_3$ in the precipitates. As the amount of NH_4OH exceeded 16.96 ml, the percentage of Mg^{2+} and Ca^{2+} recovered reached a plateau due to the equilibrium reached in the supernatant liquid.

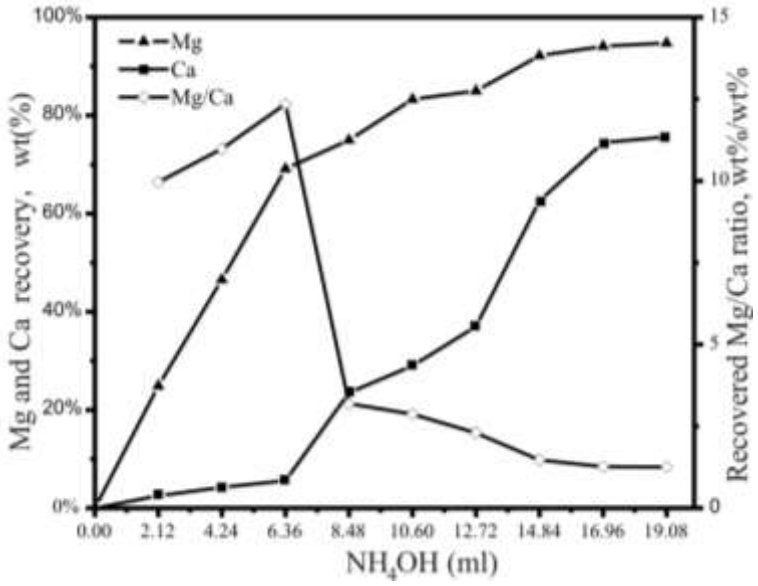

Fig. 3. Percentage of Mg^{2+} and Ca^{2+} sequestrated from reject brine as a function of NH_4OH dosage

The Mg^{2+}/Ca^{2+} ratio was also used as an indicator of the purity level of the resulting $Mg(OH)_2$ precipitates. As seen in Fig. 3, Mg^{2+}/Ca^{2+} peaked at about 12.5 when 6.36 ml of NH_4OH was added into the reject brine. This was because the initial pH was lower than 10.3, the formation of carbonates was prevented, therefore reducing the supersaturation for $CaCO_3$ and contributing to a lower precipitation of $CaCO_3$ in the solution. Therefore, a NH_4OH to Mg^{2+}

ratio of 6 was determined as the most optimum ratio out of the different values used in this study for the precipitation of $Mg(OH)_2$, which was further calcined to produce reactive MgO with a high purity.

3.3. Characterization of the synthesized $Mg(OH)_2$

3.3.1. XRD

Fig. 4 shows the XRD diffractograms of synthesized $Mg(OH)_2$ obtained from the reaction between reject brine and different amounts of NH_4OH. The crystalline peaks observed were mainly attributed to $Mg(OH)_2$ along with smaller amounts of $CaCO_3$, which was present in the crystal form of aragonite. The presence of Mg^{2+} in the reject brine inhibited the precipitation of calcite and favoured the formation of aragonite, which was in line with the findings of earlier studies (Berner, 1975). As shown in Fig. 4, the relative intensity of the peaks corresponding to $Mg(OH)_2$ and $CaCO_3$ varied as the amount of NH_4OH increased, which reflected the changes in the crystallinity and chemical composition of the precipitants. The relative intensity of the peaks corresponding to $CaCO_3$ increased along with the increasing amount of NH_4OH, which indicated the increased content percentage of $CaCO_3$ in the precipitants.

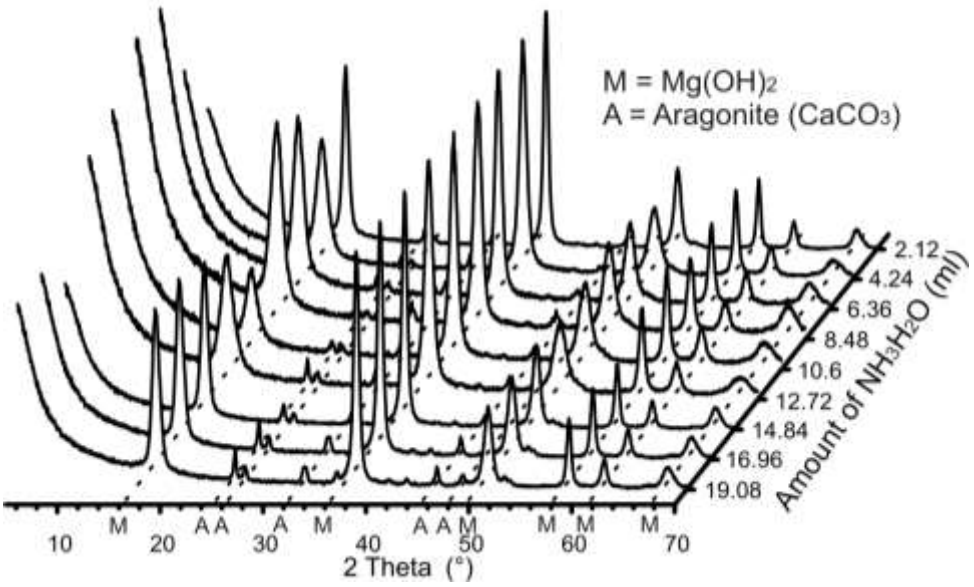

Fig. 4. XRD diffractograms of $Mg(OH)_2$ obtained from the reaction of 200 ml reject brine with different amounts of NH_4OH

3.3.2. FESEM

The morphologies of the synthesized $Mg(OH)_2$ obtained with the addition of different amounts of NH_4OH are shown in Fig. 5. A flake-like morphology with an average agglomerate size of 10-15 μm was observed in all cases, similar to the findings reported earlier in literature (Alvarado et al., 2000; Behij et al., 2013; Guo et al., 2015). As shown in the Fig. 5, the amount of NH_4OH did not have a significant influence on the morphology of $Mg(OH)_2$ synthesized from reject brine.

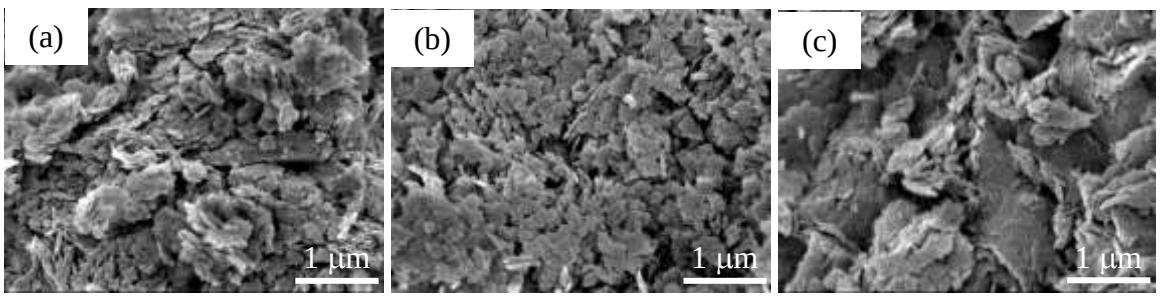

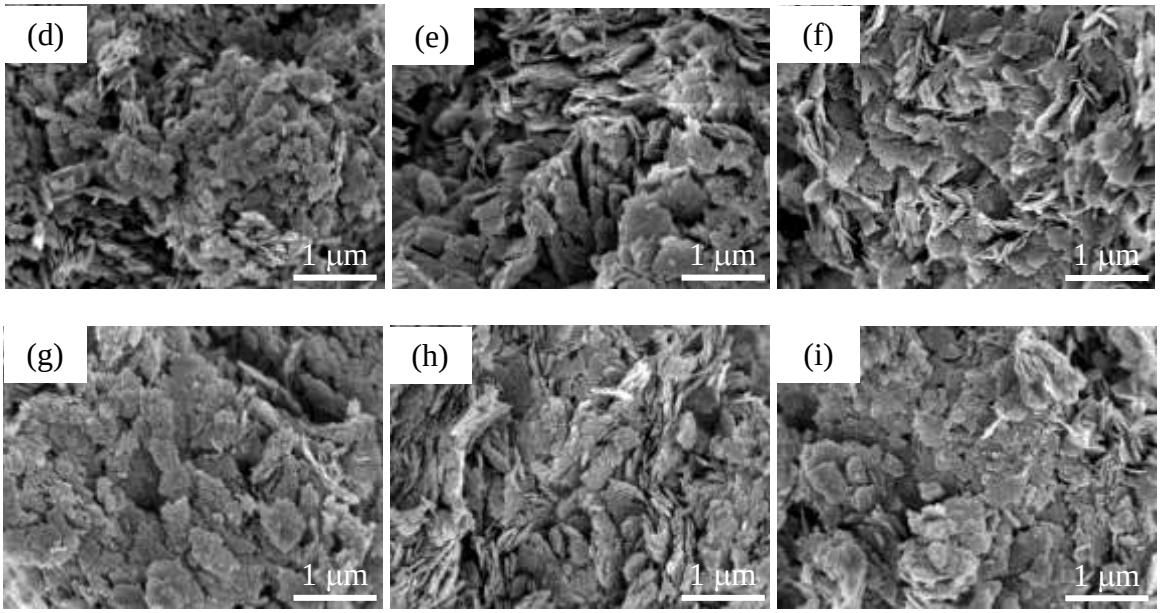

Fig. 5. FESEM images of $Mg(OH)_2$ obtained from the reaction of 200 ml reject brine with (a) 2.12, (b) 4.24, (c) 6.36, (d) 8.48, (e) 10.6, (f) 12.72, (g) 14.84, (h) 16.96 and (i) 19.08 ml of NH_4OH

3.3.3. TG/DTA

Fig. 6 illustrates a typical TG/DTA graph of the synthesized $Mg(OH)_2$ obtained by adding 6.36 ml of NH_4OH to react with the reject brine. The dehydration of $Mg(OH)_2$ took place between 340 and 440 °C and resulted in a weight loss of around 25.5% due to the loss of H_2O from the system. The second reaction, attributed to the decarbonation of $CaCO_3$, which led to the release of CO_2, was observed between 650 and 750 °C, resulting in a weight loss of 2.5%.

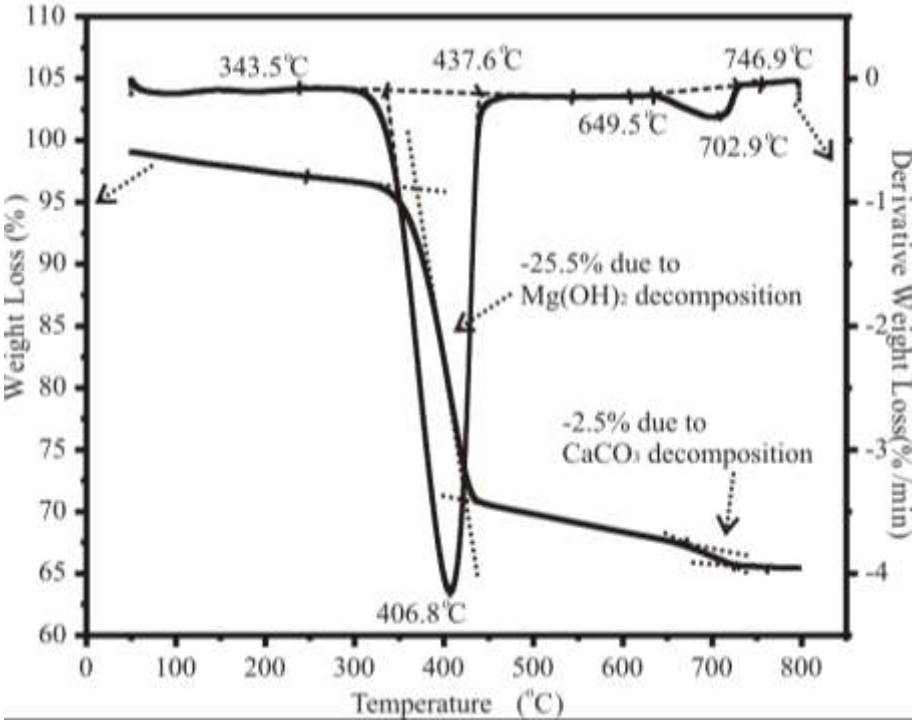

Fig. 6. Typical TG/DTA curve of $Mg(OH)_2$ obtained from the reaction of 200 ml reject brine with 6.36 ml of NH_4OH

Table 2 summarizes the peak temperatures observed during the thermal decomposition of $Mg(OH)_2$ and corresponding weight losses at each reaction. The weight loss due to the dehydration of $Mg(OH)_2$ (i.e. between 340 and 440 °C) showed a decreasing trend, while the weight loss due to the decarbonation of $CaCO_3$ (i.e. between 650 and 750 °C) increased with the amount of NH_4OH. The peak temperature at which $CaCO_3$ decomposed into CaO and CO_2 increased significantly from 655.4 to 747.2 °C with the increase in the amount of NH_4OH. This could be attributed to the poorly crystalline structure of $CaCO_3$ that formed when lower amounts of NH_4OH were reacted with the reject brine (Johnson, 2002). This was consistent with the XRD patterns shown earlier in Fig. 4, where sharper and narrower $CaCO_3$ peaks were detected under higher NH_4OH dosages.

366 Table 2 TG/DTA results of $Mg(OH)_2$ obtained from the reaction of 200 ml reject brine with
367 different amounts of NH_4OH

NH_4OH (ml)	1st peak temperature (°C)	Weight loss between 340-440°C (%)	2nd peak temperature (°C)	Weight loss between 650-750°C (%)
2.24	391.3	24.9	655.4	0.7
4.24	393.4	24.2	691.0	1.3
6.36	406.8	25.5	702.9	2.5
8.48	393.4	25.1	691.0	1.5
10.6	407.3	25.3	706.9	2.2
12.72	408.9	24.5	706.9	2.9
14.84	409.8	23.8	738.1	4.0
16.96	403.8	23.0	725.4	4.9
19.08	405.8	20.0	747.2	9.2

368

369 Table 3 lists the compositions of the synthesized $Mg(OH)_2$, which were calculated according
370 to the TG/DTA results listed in Table 2 as well as the ICP-OES results shown in Fig. 3. Both
371 measurements revealed similar trends, which indicated a decrease in the amount of $Mg(OH)_2$
372 accompanied with an increase in the amount of $CaCO_3$ as the amount of NH_4OH increased.
373 According to the result of TGA, the synthesized $Mg(OH)_2$ achieved up to 98% in purity when
374 2.24 ml of NH_4OH was added into the reject brine. While ICP-OES test indicated the highest
375 purity of $Mg(OH)_2$ of 97.3% was achieved when 6.36 ml of NH_4OH was added. However,
376 low dosages of NH_4OH cannot achieve the supersaturation for the formation of $Mg(OH)_2$,
377 leading to a lower yield of precipitates. As such, a NH_4OH to Mg^{2+} ratio of 6 at a NH_4OH
378 content of 6.36 ml, which led to a Mg^{2+} yield of 70% (Fig. 3) and a $Mg(OH)_2$ with a purity of
379 93.5% (Table 3), was chosen for the large scale production of $Mg(OH)_2$, which was then
380 calcined to produce reactive MgO.

381

382 Table 3 Chemical composition of the synthesized $Mg(OH)_2$ based on TG/DTA and ICP-OES
383 results

NH_4OH (ml)	TG/DTA		ICP-OES	
	$Mg(OH)_2$ (%)	$CaCO_3$ (%)	$Mg(OH)_2$ (%)	$CaCO_3$ (%)
2.24	98.0	2.0	96.6	3.4
4.24	96.4	3.6	96.9	3.1
6.36	93.5	6.5	97.3	2.7
8.48	95.9	4.1	90.2	9.8
10.6	94.2	5.8	89.2	10.8
12.72	92.4	7.6	86.9	13.1
14.84	89.5	10.5	80.9	19.1
16.96	87.0	13.0	78.4	21.6
19.08	75.6	24.4	78.3	21.7

3.4. Characterization of the synthesized reactive MgO

3.4.1. XRD

The $Mg(OH)_2$ obtained at a NH_4OH to Mg^{2+} ratio of 6 was calcined at 500 °C for 2 hours in a furnace for the production of reactive MgO, whose XRD patterns are shown in Fig. 7. The main peak positions of the synthesized reactive MgO matched well with the reference peaks of MgO (JCPDS # 89-7746) with few minor peaks attributed to the presence of calcite, which may have formed from the transformation of aragonite at higher temperatures (Kontoyannis and Vagenas, 2000). The lack of $Mg(OH)_2$ peaks was an indication that all the initially used brucite fully decomposed at the calcination conditions used (i.e. 500 °C for 2 hours), resulting in the formation of reactive MgO.

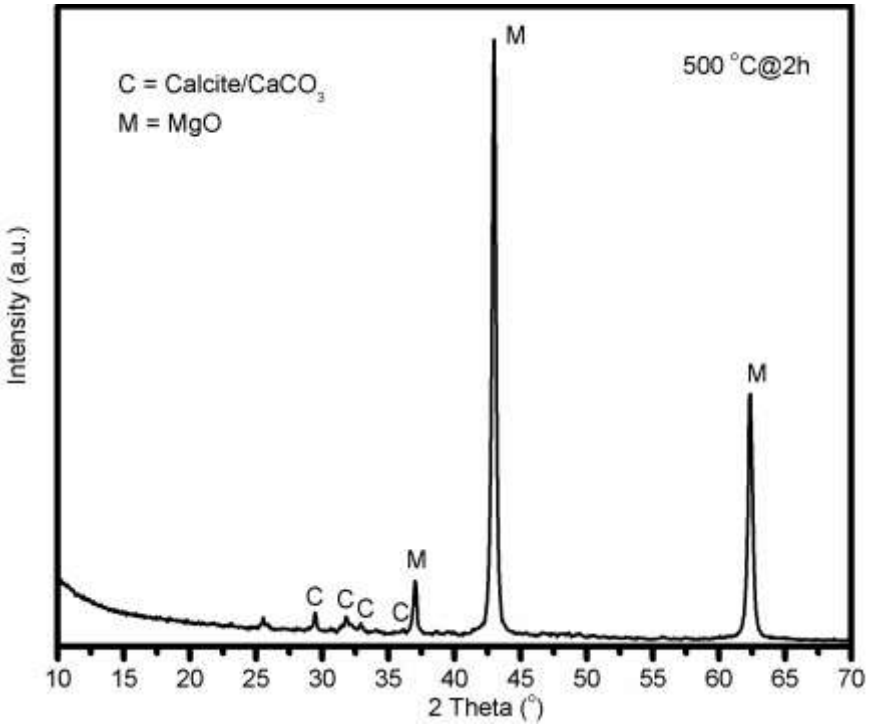

Fig. 7. XRD diffractograms of the produced reactive MgO

3.4.2. FESEM

Figs. 8(a) and (b) illustrate the morphology of the reactive MgO produced from the calcination of $Mg(OH)_2$ at 500 °C. A plate-like morphology, which was inherited from the parent material brucite as was shown in Fig. 5, was observed throughout the microstructure of MgO. Different from the closely packed structure of brucite, MgO demonstrated a more porous structure due to the loss of water molecules during the decomposition of brucite into MgO. This finding was in agreement with previous studies (Alvarado et al., 2000; Mo et al., 2010), in which the porous plate-like morphology of MgO calcined from magnesite was reported. The main difference between the morphology shown in Fig. 8 and those reported in relevant literature was the much smaller particle size of the MgO grains in the former due to the low calcination temperature (500 °C) utilized in its production.

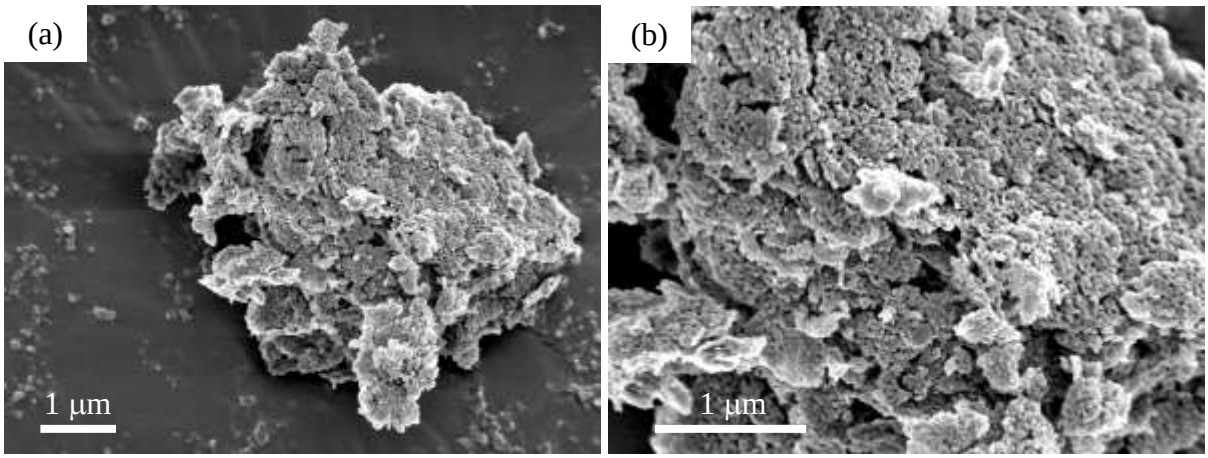

Fig. 8. FESEM images of the reactive MgO produced at 500 °C at different magnifications of (a) x14,000 and (b) x30,000

3.4.3. BET

Fig. 9 presents a comparison between the SSA values of the reactive MgO obtained from reject brine in this study and 12 different commercial MgO samples presented in an earlier study (Jin and Al-Tabbaa, 2014). The synthesized reactive MgO, referred to as "SRM", achieved a SSA of 78.8 m^2/g, which was higher than the SSA of most of the MgO samples obtained via the dry route (i.e. through the calcination of magnesite). Alternatively, the SRM revealed a lower SSA when compared to the MgO samples obtained via synthetic routes. This could be attributed to the higher impurity level of SRM (90.8%) compared to the commercial synthetic MgO samples (e.g. DSP (99.2%) and N50 (97.7%)). The presence of the main impurity $CaCO_3$, who also possessed a low SSA, have also contributed to the generally lower reactivity of SRM amongst the synthetically produced MgO samples.

Regardless of the different SSA comparisons, the SRM obtained in this study can be classified under "category I" referring to highly reactive MgO with an SSA of over 60 m^2/g according to the classification of reactive MgO proposed by (Jin and Al-Tabbaa, 2014).

Furthermore, it must be kept in mind that the SSA and therefore the reactivity of the MgO synthesized from the reject brine as presented in this study can be further increased with an optimization of production conditions.

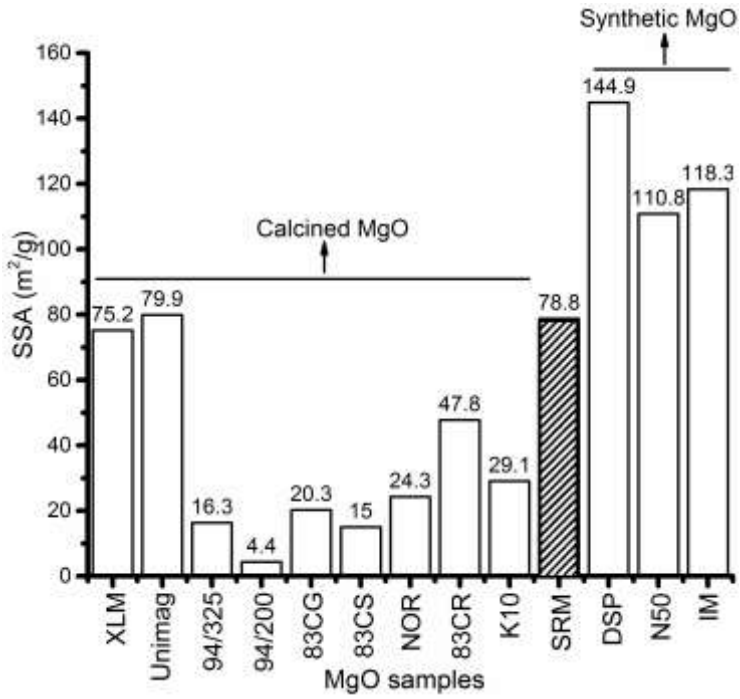

Fig. 9. SSA of the synthesized reactive MgO (SRM) compared with 12 commercial MgO samples reported in (Jin and Al-Tabbaa, 2014)

4. Conclusions

This study shed light on the significant potential of reject brine in the recovery of Mg^{2+} and the synthesis of reactive MgO with a wide range of potential applications. The obtained results demonstrated the feasibility of synthesizing reactive MgO from reject brine obtained from a desalination plant. NH_4OH was used as alkali source to precipitate $Mg(OH)_2$ from reject brine. The influence of the amount of NH_4OH was investigated to optimize the yield and increase the purity of the precipitates. An optimum NH_4OH to Mg^{2+} ratio of 6, which

resulted in a high Mg content while minimizing Ca-based impurities, was determined. This led to the synthesis of $Mg(OH)_2$ with a high purity of 93.5%, which was further calcined at 500 °C for 2 hours to produce highly reactive MgO with a SSA of 78.8 m^2/g. A comparison of the produced MgO with commercially available reactive MgO samples indicated its capability to be used in different applications necessitating the use of reactive MgO with a high SSA.

Acknowledgements

This project is funded by the National Research Foundation (NRF), Prime Minister's Office, Singapore under its Campus for Research Excellence and Technological Enterprise (CREATE) program.

References

Adham, S., Hussain, A., Matar, J.M., Dores, R. and Janson, A., 2013. Application of membrane distillation for desalting brines from thermal desalination plants. Desalination, 314: 101-108.

Ahmed, M., Arakel, A., Hoey, D., Thumarukudy, M.R., Goosen, M.F.A., Al-Haddabi, M. and Al-Belushi, A., 2003. Feasibility of salt production from inland RO desalination plant reject brine: a case study. Desalination, 158(1-3): 109-117.

Al-Tabbaa, A., 2013. Reactive magnesia cement. In: F. PachecoTorgal, S. Jalali, J. Labrincha and V.M. John (Eds.), Eco-Efficient Concrete. Woodhead Publishing, pp. 523-543.

Al-Zahrani, A. and Abdel-Majeed, M., 2007. Production of magnesia from local dolomite ores and rejected brines from local desalination plants, Saudi Engineering Conference.

467 Alvarado, E., Torres-Martinez, L.M., Fuentes, A.F. and Quintana, P., 2000. Preparation and
468 characterization of MgO powders obtained from different magnesium salts and the
469 mineral dolomite. Polyhedron, 19(22-23): 2345-2351.
470 Bartley, J.K., Xu, C.L., Lloyd, R., Enache, D.I., Knight, D.W. and Hutchings, G.J., 2012.
471 Simple method to synthesize high surface area magnesium oxide and its use as a
472 heterogeneous base catalyst. Applied Catalysis B-Environmental, 128: 31-38.
473 Behij, S., Hammi, H., Hamzaoui, H. and M'nif, A., 2013. Magnesium salts as compounds of
474 the preparation of magnesium oxide from Tunisian natural brines. Chemical Industry
475 and Chemical Engineering Quarterly, 19(2): 263-271.
476 Berner, R.A., 1975. The role of magnesium in the crystal growth of calcite and aragonite from
477 sea water. Geochimica et Cosmochimica Acta, 39(4): 489-504.
478 Caraballo, M.A., Rotting, T.S., Macias, F., Nieto, J.M. and Ayora, C., 2009. Field multi-step
479 limestone and MgO passive system to treat acid mine drainage with high metal
480 concentrations. Applied Geochemistry, 24(12): 2301-2311.
481 Choudhary, V.R., Rane, V.H. and Gadre, R.V., 1994. Influence of Precursors Used in
482 Preparation of MgO on Its Surface Properties and Catalytic Activity in Oxidative
483 Coupling of Methane. Journal of Catalysis, 145(2): 300-311.
484 Dave, R.H. and Ghosh, P.K., 2005. Enrichment of bromine in sea-bittern with recovery of
485 other marine chemicals. Industrial & Engineering Chemistry Research, 44(9): 2903-
486 2907.
487 El-Naas, M.H., 2011. Reject brine management. Desalination, Trends and Technologies,
488 Croatia, InTech: 237-252.
489 Eubank, W.R., 1951. Calcination studies of magnesium oxides. Journal of the American
490 Ceramic Society, 34(8): 225-229.

491 Friedrich, R., Robinson, H. and Spencer, R., 1946. Magnesium hydroxide from sea water.
492 Google Patents.
493 Gao, P., Lu, X., Geng, F., Li, X., Hou, J., Lin, H. and Shi, N., 2008. Production of MgO-type
494 expansive agent in dam concrete by use of industrial by-products. Building and
495 Environment, 43(4): 453-457.
496 Guo, H., Pei, Y., Wang, Z., Yang, Y., Wang, K., Xie, J. and Liu, Y., 2015. Preparation of
497 $Mg(OH)_2$ with caustic calcined magnesia through ammonium acetate circulation.
498 Hydrometallurgy, 152: 13-19.
499 Hassan, D., 2013. Environmental sustainability assessment & associated experimental
500 investigatations of magnesia production routes, PhD Thesis, University of Cambridge.
501 Henrist, C., Mathieu, J.-P., Vogels, C., Rulmont, A. and Cloots, R., 2003. Morphological
502 study of magnesium hydroxide nanoparticles precipitated in dilute aqueous solution.
503 Journal of Crystal Growth, 249(1): 321-330.
504 Hyflux, 2011. Pollution control study for Tuas desalination and power plant project,
505 TuasSpring Pte Ltd.
506 IDA, 2015. The current state of desalination. International Desalination Association.
507 Itatani, K., Koizumi, K., Howell, F.S., Kishioka, A. and Kinoshita, M., 1988. Agglomeration
508 of magnesium oxide particles formed by the decomposition of magnesium hydroxide.
509 Part 1: Agglomeration at increasing temperature. Journal of Materials Science, 23(9):
510 3405-3412.
511 Jin, F. and Al-Tabbaa, A., 2014. Characterisation of different commercial reactive magnesia.
512 Advances in Cement Research, 26(2): 101-113.
513 Johnson, D.A., 2002. Metals and chemical change. Royal Society of Chemistry.

514 Khuyen Thi, T., Han, K.S., Kim, S.J., Kim, M.J. and Tam, T., 2016. Recovery of magnesium
515 from Uyuni salar brine as hydrated magnesium carbonate. Hydrometallurgy, 160: 106-
516 114.
517 Kontoyannis, C.G. and Vagenas, N.V., 2000. Calcium carbonate phase analysis using XRD
518 and FT-Raman spectroscopy. The Analyst, 125(2): 251-255.
519 Kramer, D.A., 2001. Magnesium, its alloys and compounds. Industrial Minerals and Rocks.
520 Lee, E.K., Jung, K.D., Joo, O.S. and Shul, Y.G., 2004. Magnesium oxide as an effective
521 catalyst in catalytic wet oxidation of H2S to sulfur. Reaction Kinetics and Catalysis
522 Letters, 82(2): 241-246.
523 Liska, M., Al-Tabbaa, A., Carter, K. and Fifield, J., 2012a. Scaled-up commercial production
524 of reactive magnesium cement pressed masonry units. Part I: Production. Proceedings
525 of the Institution of Civil Engineers-Construction Materials, 165(4): 211-223.
526 Liska, M., Al-Tabbaa, A., Carter, K. and Fifield, J., 2012b. Scaled-up commercial production
527 of reactive magnesia cement pressed masonry units. Part II: Performance. Proceedings
528 of the Institution of Civil Engineers-Construction Materials, 165(4): 225-243.
529 Mo, L.W., Deng, M. and Tang, M.S., 2010. Effects of calcination condition on expansion
530 property of MgO-type expansive agent used in cement-based materials. Cement and
531 Concrete Research, 40(3): 437-446.
532 Mo, L.W., Deng, M., Tang, M.S. and Al-Tabbaa, A., 2014. MgO expansive cement and
533 concrete in China: Past, present and future. Cement and Concrete Research, 57: 1-12.
534 Mohamed, A.M.O., Maraqa, M. and Al Handhaly, J., 2005. Impact of land disposal of reject
535 brine from desalination plants on soil and groundwater. Desalination, 182(1-3): 411-
536 433.

Pankratz, T., 2004. An overview of seawater intake facilities for seawater desalination. The Future of Desalination in Texas, 2.

PUB, 2015. The Singapore water story. Public Utilities Board.

RAM, 2015. Global magnesium oxide industry report 2015 - Forecasts to 2020. Research and Markets.

Shand, M.A., 2006. The chemistry and technology of magnesia. John Wiley & Sons.

Sillén, L.G., Martell, A.E. and Bjerrum, J., 1964. Stability constants of metal-ion complexes. Chemical Society.

Tran, K.T., Van Luong, T., An, J.W., Kang, D.J., Kim, M.J. and Tran, T., 2013. Recovery of magnesium from Uyuni salar brine as high purity magnesium oxalate. Hydrometallurgy, 138: 93-99.

Turek, M. and Gnot, W., 1995. Precipitation of magnesium hydroxide from brine. Industrial & Engineering Chemistry Research, 34(1): 244-250.

Unluer, C. and Al-Tabbaa, A., 2013. Impact of hydrated magnesium carbonate additives on the carbonation of reactive MgO cements. Cement and Concrete Research, 54: 87-97.

Unluer, C. and Al-Tabbaa, A., 2014. Enhancing the carbonation of MgO cement porous blocks through improved curing conditions. Cement and Concrete Research, 59: 55-65.

Wang, Z., Wang, N.H., Li, T. and Cao, Y., 2012. 3D numerical analysis of the arc plasma behavior in a submerged DC electric arc furnace for the production of fused MgO. Plasma Sci. Technol., 14(4): 321-326.

Yan, C., Xue, D., Zou, L., Yan, X. and Wang, W., 2005. Preparation of magnesium hydroxide nanoflowers. Journal of Crystal Growth, 282(3): 448-454.